Potassium effect in K-Ni(Co)PW/Al$_2$O$_3$ catalysts for selective hydrotreating of model FCC gasoline

D. Ishutenko [a], P. Minaev [a], Yu. Anashkin [a], M. Nikulshina [a], A. Mozhaev [a], K. Maslakov [b], P. Nikulshin [a,*]

[a] *Samara State Technical University, 244 Molodogvardeiskaya St., Samara 443100, Russia*
[b] *Chemistry Department, M.V. Lomonosov Moscow State University, 1-3 Leninskiye Gory, Moscow 119991, Russia*

ARTICLE INFO

ABSTRACT

Ni(Co)-PW/Al$_2$O$_3$ catalysts both unmodified and modified with potassium were synthesized with the use of H$_3$PW$_{12}$O$_{40}$, CoCO$_3$ or NiCO$_3$, KOH and citric acid. The catalysts were characterized by the techniques such as low-temperature N$_2$ adsorption, temperature-programmed reduction, X-ray photoelectron spectroscopy, and high-resolution transmission electron microscopy. The prepared samples were tested in hydrotreating of model FCC gasoline that contained 1000 ppm of sulfur from thiophene and 36 wt.% of *n*-hexene-1 as a representative olefinic compound. The modification with an alkali metal influenced both the characteristics of the catalyst active phase and catalytic properties of (K)-Ni(Co)-PW/Al$_2$O$_3$ samples. The incorporation of potassium led to some l growth of the linear size of active phase crystallites, to a decrease of reactivity and of the number of active sites, to a strong decrease of CoWS and NiWS particle amounts with a simultaneous rise of separate CoS$_x$ and NiS$_x$. The potassium addition also induced a drastic drop of hydrodesulfurization (HDS) and hydrogenation (HYDO) activity with a HDS/HYDO selectivity decrease for Ni- and Co-promoted systems and with a significant increase of the selectivity factor for unpromoted PW/Al$_2$O$_3$. The Ni-promoted catalyst proved to be more sensitive to the potassium modification than the Co-promoted one. So, the modified catalysts can be ranged by activity as follows: KWS < KNiWS « CoS$_x$ + KWS. A key factor for selecting a catalyst was shown to be the chemical composition of FCC gasoline: feeds with a high sulfur amount required NiWS systems, whereas low sulfur feeds with a great amount of olefins should be hydrotreated with KCoMoS formulations.

© 2016 Elsevier B.V. All rights reserved.

1. Introduction

Gasoline is one of the most expendable petroleum products today. It is produced by blending of various fractions from different downstream processes such as catalytic reforming, alkylation, isomerization, and fluid catalytic cracking (FCC). The FCC product accounts for the major part of commercial gasoline. It is well known that FCC gasoline is characterized by a high amount of sulfur compounds [1], what makes it a main sulfur contributor to the gasoline pool. As a result, commercial petrol cannot meet current strict environmental standards. The solution is to refine FCC gasoline before blending. It is unreasonable to operate the traditional hydrotreating (HDT) process with common sulfide Co(Ni)Mo(W) catalysts. FCC gasoline contains a large amount of olefin hydrocarbons—up to 40 wt.% [1] characterized by a high research octane number (RON)

and propensity to saturation during conventional HDT. As a result, such upgraded FCC gasoline greatly loses in RON. Therefore, it is quite a challenge to design a well-balanced catalyst for hydrodesulfurization (HDS) and olefin hydrogenation (HYDO) reactions.

Typical catalysts for hydro-upgrading of petroleum fractions are Co- or Ni-promoted MoS$_2$ and WS$_2$. A choice of the catalytic composition type strongly depends on the feed type. For instance, W-based catalysts are known for their application in various refinery processes: production of ULSD [2–5], HDT and hydrocracking of heavy oil fractions [6–10], and production of biofuels from spent cooking [11,12] and vegetable oils [13–15]. Moreover, there is a number of publications concerning the use of W-based catalysts in HDT of FCC gasoline [16,17], although they are rare and not systematic. Kordulis et al. [16] studied a new pathway to prepare a NiW catalyst supported on γ-Al$_2$O$_3$ for HDS of FCC gasoline. The authors synthesized samples by the modified equilibrium deposition filtration (MEDF) and conventional non-dry impregnation (NDI) and compared them with each other and with a commercial CoMo catalyst. The novel catalyst gained activity of the commer-

cial sample in the sulfur removal and olefin saturation whereas the NiW-MEDF sample exhibited slightly higher isomerization activity than the commercial analog. The RON loss calculated for the test with the novel NiW/γ-Al$_2$O$_3$ catalyst was slightly less than that with the commercial sample, though still high—7.88. Lower HYDO activity (∼87%) was found with the NiW-NDI sample, its HDS activity being also the lowest. The authors concluded that milder process conditions would help achieve a satisfactory HDS degree and olefin saturation with the minimum RON loss for the NiW-MEDF catalyst. Shan et al. [17] have also proposed a novel method for synthesizing NiW catalysts for selective HDT of FCC gasoline. The key factor to adjust high HDS with low HYDO activities was a possibility to tune up the size and morphology of particles with the new preparation technique. The best HDS/HYDO selectivity factor was reached over a catalyst with the active phase species characterized by a smaller size, higher stacking number and optimized Ni loading. The results let the authors presume that the new method of catalyst preparation from W-based hybrid nanocrystals allowed avoiding the formation of aluminoheteropolytungstates that could further transform to bulk WO$_3$ crystallites and the Al$_2$(WO$_4$)$_3$ phase and then to low-dispersed (Ni)WS species. Also, the described approach permitted preserving the W species dispersion and forming NiWS active phase particles with a lower brim to the edge site ratio. However, the RON loss that occurred with the novel catalysts remained high and varied in a range from 2.5 to 4.9.

The use of W-based catalysts for hydro-upgrading of FCC gasoline has not been investigated enough and may hold promise. The active phase of Ni(Co)WS catalysts is similar to that of Co(Ni)MoS and is represented as WS$_2$ crystallites whose edges are decorated with promoter atoms having alike morphology [18–20]. It is considered that Co-promoted WS$_2$ catalysts are not as active as Ni-promoted ones [21,22]. For this reason, CoWS catalysts are not widespread in industry. Moreover, NiW-supported samples usually are less active in HDS reactions than Co(Ni)Mo systems [23]. The main difference between W- and Mo-based catalysts is a propensity to sulfidation. Catalysts synthesized from tungsten-containing precursors undergo strong sulfidation with formation of a great amount of oxysulfides and separate NiS$_x$. Therefore, to obtain a higher content of the NiWS active phase more severe conditions such as higher temperature and hydrogen pressure are required in comparison with Mo-based catalysts [24]. Furthermore, W atoms were found to tend to a strong interaction with the support (usually γ-Al$_2$O$_3$), what appeared a great limiting factor for NiWS active phase formation [25]. To obtain a highly active W-based catalyst the following methods are usually employed: (i) novel support with a low propensity to formation of bonds with W atoms: ZrO$_2$, TiO$_2$, γ-alumina nanorod, and SiO$_2$-Al$_2$O$_3$ [7,26–29]; (ii) chelating agents for improving selective formation of NiWS species: citric acid, NTA, EDTA, and CyDTA [4,30–35]; (iii) new precursors such as heteropolytungstates and heteropolyacids [25,36–45]; (iv) advanced syntheses such as the modified equilibrium deposition filtration, hybrid nanocrystals-assisted hydrothermal deposition, grafting and the deposition of Ni and W molecular precursors onto the support, and the microwave hydrothermal method [16,17,46,47].

Taking into account that W-based catalysts are famous primarily for their high hydrogenation activity [44–50], it is unreasonable to use such catalytic systems in selective HDT of FCC gasoline without suppressing their activity to olefin saturation. Recently, we have discovered a beneficial effect of potassium on HDS/HYDO selectivity of CoMo catalysts prepared using 12-molybdophosphoric heteropolyacid H$_3$PMo$_{12}$O$_{40}$ [51,52]. The modification with an alkali metal led to a drastic decrease of HYDO activity with a simultaneous small reduction of HDS activity, which was explained by the potassium impact primarily on HYDO active sites. The same approach was chosen in the current research. This study aims at investigating the potassium modification impact on the active phase characteristics and catalytic properties of (K)-Ni(Co)-PW/Al$_2$O$_3$ catalysts synthesized with the use of 12-tunstophosphoric heteropolyacid H$_3$PW$_{12}$O$_{40}$ in HDT of model FCC gasoline containing thiophene and n-hexene-1.

2. Experimental

2.1. Catalyst preparation

Unmodified and K-modified samples were synthesized with a view to investigate the alkali metal modifier impact on activity and selectivity of Ni(Co)-PW/Al$_2$O$_3$ catalysts. H$_3$PW$_{12}$O$_{40}$, CoCO$_3$, NiCO$_3$, KOH, and citric acid (CA) (all reagents from Sigma-Aldrich, p.a.) were used as precursors. Catalysts were prepared by pore-volume impregnation of the support with joint aqueous solutions containing the required quantities of active components. γ-Al$_2$O$_3$ with the specific surface area (SSA) 218 m^2/g, pore volume 0.64 cm^3/g and effective pore radius 48 Å was used as a support. The K-Ni(Co)-PW/Al$_2$O$_3$ samples were modified with 7.5 wt.% alkali metal. The preparation procedure was as follows. A mechanical mixture of CA and CoCO$_3$ or NiCO$_3$ (CA/Co(Ni) molar ratio = 1) was dissolved in deionized water. H$_3$PW$_{12}$O$_{40}$ was dissolved in hot deionized water in a separate beaker and heated to 60–80 °C with stirring until the acid completely dissolved. Next, the promoter citrate solution was added to the acid solution with subsequent cooling down. For the modified catalysts, KOH was also slowly added to the joint solution. The pH value of the joint solution was in the range of 3–4. Subsequently, the dried alumina was impregnated with the prepared solutions and aged overnight at room temperature. After aging, the solids were dried at 110 °C for 6 h. The K$_2$S/Al$_2$O$_3$ sample with 7.5 wt% potassium was prepared as a reference sample via alumina impregnation with the aqueous solution of KOH and CA with further drying and sulfidation. An EDX800HS analyzer was used to determine the exact amount of loaded metals. The chemical composition and textural characteristics of the synthesized catalysts are summarized in Table 1.

2.2. Characterisation of catalysts

The prepared oxidic samples were sulfided to analyze the catalysts in the active state. The activation was performed by heating in a hydrogen flow with a mixture of dimethyldisulfide (DMDS, 2 wt.% sulfur) in n-heptane. First, the samples were heated up to 240 °C over the holding period of 10 h and then the temperature was raised up to 340 °C to be kept as such over 6 h. To determine the textural properties of the synthesized catalysts the low-temperature nitrogen adsorption on a Quantachrome Autosorb-1 adsorption porosimeter was performed. The specific surface area was estimated with the use of BET methodology and the total pore volume and pore size distribution were calculated from the desorption curve in the BJH model.

To define the geometrical characteristics of the catalyst active phase the HRTEM images were recorded using a Tecnai G2 20 electron microscope and analyzed by the Fourier method. For each catalyst, about 10–15 representative high-resolution microphotographs with more than 400 slabs were studied. According to [53] WS$_2$ slabs can be assumed to be perfect hexagons, what allowed to calculate the dispersion of (K)WS$_2$ and (K)-Ni(Co)WS particles, the edge-to-corner ratio of WS$_2$ slabs and other geometrical properties. Thus, the active phase dispersion was calculated as follows:

$$D = \frac{W_e + W_c}{W_T} = \frac{\sum_{i=1..t} 6n_i - 6}{\sum_{i=1..t} 3n_i{}^2 - 3n_i + 1}, \tag{1}$$

Table 1
Chemical composition and textural characteristics of synthesized (K)-PW/Al$_2$O$_3$ and (K)-Ni(Co)-PW/Al$_2$O$_3$ catalysts.

Catalyst	Content (wt.%)				Textural characteristics		
	Co	Ni	W	K	SSA[a](m^2 g^{-1})	PV[b](cm^3 g^{-1})	AD[c](Å)
PW/Al$_2$O$_3$	–	–	20.1	–	173	0.39	48
CA-PW/Al$_2$O$_3$	–	–	20.2	–	161	0.33	48
K-PW/Al$_2$O$_3$	–	–	19.9	7.4	148	0.36	48
Co-PW/Al$_2$O$_3$	3.2	–	19.6	–	137	0.30	47
Ni-PW/Al$_2$O$_3$	–	3.1	19.5	–	131	0.31	47
K-Co-PW/Al$_2$O$_3$	3.1	–	19.7	7.5	134	0.27	47
K-Ni-PW/Al$_2$O$_3$	–	3.1	19.8	7.5	129	0.27	47

[a] Specific surface area.
[b] Pore volume.
[c] Average pore diameter.

where W_e is the total number of W atoms at the edge surface, W_c is the number of corner W atoms, W_T is the total number of W atoms, n_i is the number of W atoms along one side of the WS$_2$ slab, as determined by its length, and t is the total number of slabs in the TEM micrograph.

The average stacking number ($\overline{N}$) was determined as the number of slabs per stack:

$$\overline{N} = \frac{\sum_{i=1..t} n_i N_i}{\sum_{i=1..t} n}, \qquad (2)$$

where n_i is the number of stacks in N_i layers.

The edge-to-corner ratio of the WS$_2$ slab $(f_e/f_c)_W$ was derived according to [43,44]:

$$(f_e/f_c)_W = \frac{W_e}{W_c} = \frac{10 \times \overline{L}/3.2 - 3}{2}, \qquad (3)$$

where $\overline{L}$ is the average slab length (nm) calculated as the average number of manually defined linear sizes of more than 400 slabs for each sample.

The W-S bond strength in the sulfided catalyst was estimated by temperature-programmed reduction (TPR). Before the analysis, the samples were sulfided with the mixture of 10 vol.% H$_2$S in H$_2$ at 400 °C during 4 h. The TPR analyses were conducted with the mixture of 5 vol.% H$_2$ in N$_2$. TPR profiles were recorded with the use of a thermal conductivity detector (TCD) under the conditions such as the volume flow rate 25 ml/min, temperature range from room to 900 °C, holding period at 900 °C of 1 h, and the heating rate 10°/min. K$_2$S/Al$_2$O$_3$ was used as the reference sample.

The composition and chemical state of different elements on the catalyst surface were evaluated by the XPS technique. The spectra were recorded using a Kratos Axis Ultra DLD spectrometer with the monochromatic AlK$_a$ source (hn = 1486.6 eV, 150 W). The binding energy (BE) values were attributed to the positions of the Au 4f$_{7/2}$ peak at 83.96 eV and of the Cu 2p$_{3/2}$ peak at 932.62 eV. To examine the photoelectron spectra the narrow spectral regions (Al 2p, S 2p, S 2s, W 4f, C 1s, K 2p, O 1s, Co 2p, and Ni 2p) were recorded. The collected spectra were processed by the mixed Gaussian (30%)−Lorentzian (70%) method using the CasaXPS program. Atomic concentrations were calculated from the Shirley background subtraction. Decompositions of the S 2p, W 4f, Co 2p, and Ni 2p XPS spectra were performed using appropriate oxide and sulfided references as supported monometallic catalysts [43,44,54].

The XPS decomposition allowed calculating the absolute quantification of each species:

$$C(j)_T = \frac{A_j/S_j}{\sum_{i=1..n} A_i/S_i} \times 100, \qquad (4)$$

where A_i is the measured area of species i, S_i is the sensitivity factor of the atom related to species i (provided by the manufacturer), and $C(j)_T$ is the absolute content of species j.

Also, relative concentrations of each species, Co(Ni)$^{2+}$ in the oxide state, separate Co(Ni)S$_x$, Co(Ni)WS, tungsten oxide W^{6+}, WS$_x$O$_y$, and WS$_2$ for every sulfided catalyst were determined. For instance, the relative Co(Ni)WS amount was calculated as:

$$[Co(Ni)WS](\%) = \frac{A_{Co(Ni)WS}}{A_{Co(Ni)WS} + A_{Co(Ni)S_x} + A_{Co(Ni)^{2+}}} \times 100, \qquad (5)$$

where A_X represents the peak area of species x.

The effective Co(Ni) content in the Co(Ni)WS active phase was derived by the relation:

$$C_{Co(Ni)WS} = [Co(Ni)WS] \times C(Co(Ni))_T, \qquad (6)$$

where $C(Co(Ni))_T$ attributed to the effective concentration of cobalt (nickel) was determined by XPS (at.%).

The promotion ratio of active phase slabs was calculated by the equation:

$$(Co(Ni)/W)_{slab} = \frac{C_{Co(Ni)WS}}{C_{WS_2}} \qquad (7)$$

where C_X is the absolute Co(Ni) and W concentration in the Co(Ni)WS and WS$_2$ species, respectively (at.%).

The promoter ratio in the slab edge of the active phase was calculated as [43,44,54]:

$$(Co(Ni)/W)_{edge} = \frac{(Co(Ni)/W)_{slab}}{W_e + W_c} \times W_T = \frac{(Co(Ni)/W)_{slab}}{D}, \qquad (8)$$

where D is the dispersion of the active phase species calculated with the TEM measurements.

The edge-to-corner ratio of the Co(Ni)WS slab was obtained from the XPS and HRTEM data:

$$(f_e/f_c)_{Co(Ni)W} = (f_e/f_c)_W \times (Co(Ni)/W)_{edge} \qquad (9)$$

2.3. Catalytic properties

Catalytic activity of the synthesized samples was studied in HDT of model FCC gasoline. The following model compounds were used to prepare the feed: thiophene (1000 ppm S) as a sulfur-organic component, n-hexene-1 (36 wt.%) as a high-reactive unsaturated hydrocarbon, n-heptane as a solvent, and n-octane as an internal standard for the gas chromatography (GC) analysis. The process was held in a fixed-bed flow microreactor under the conditions:
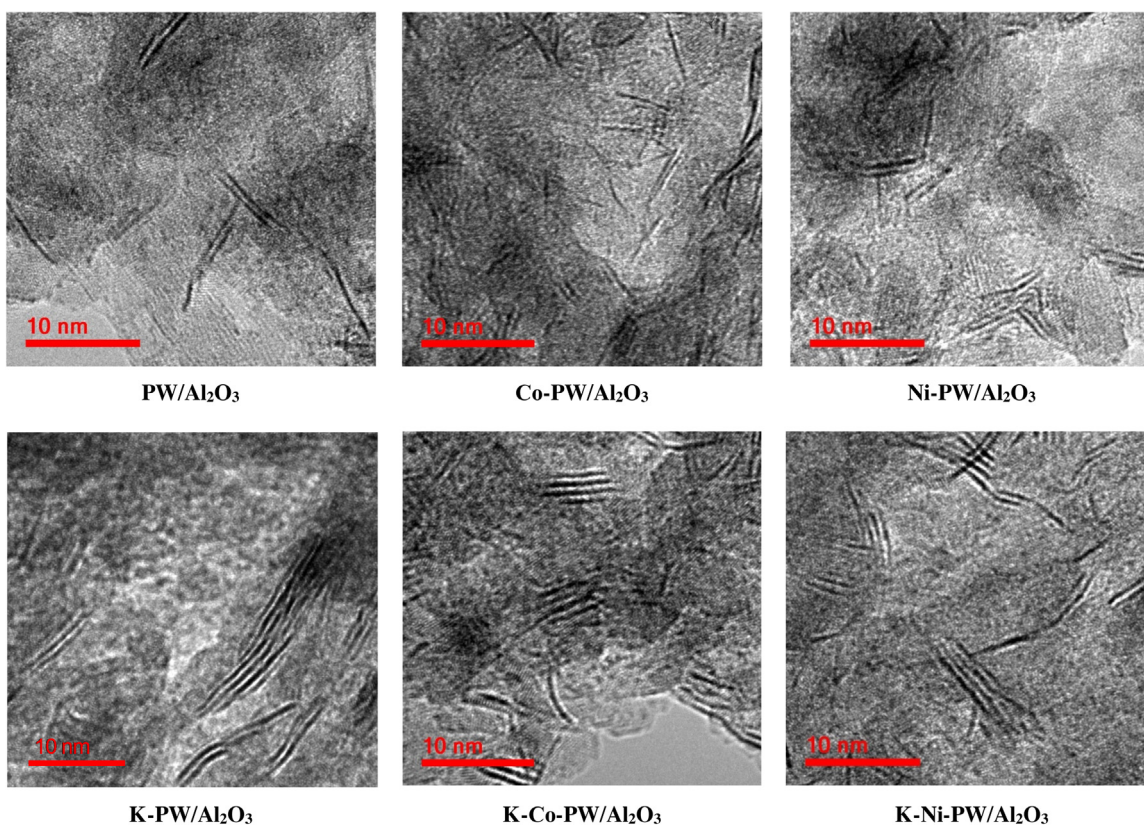
Fig. 1. HRTEM images of prepared (K)-PW/Al$_2$O$_3$ and (K)-Ni(Co)-PW/Al$_2$O$_3$ catalysts.

250 °C, 1.5 MPa of hydrogen, 5 h^{-1} liquid hourly space velocity and the 100 NL/L volume ratio of hydrogen to feed. The GC method was employed for analysing the products from the reactor.

Activity of the catalysts was estimated using HDS (the amount of reacted thiophene) and HYDO (the amount of reacted n-hexene-1) conversions as well as rate constants of the pseudo-first-order reactions and the turnover frequency number:

$$x_T(\%) = \frac{C_S^0 - C_S}{C_S^0} \times 100 \quad \text{and} \quad x_H(\%) = \frac{C_H^0 - C_H}{C_H^0} \times 100 , \quad (10)$$

where C_S^0 and C_H^0 are thiophene and n-hexene-1 contents in the feedstock (wt.%), respectively; C_S and C_H are thiophene and n-hexene-1 contents in the products (wt.%), respectively;

$$k_{HDS} = -\frac{F_T}{W} \ln(1 - x_T) \quad \text{and} \quad k_{HYD} = -\frac{F_H}{W} \ln(1 - x_H), \quad (11)$$

where k_{HDS} and k_{HYD} are pseudo-first order reaction constants of thiophene HDS and n-hexene-1 HYDO (mol g^{-1} h^{-1}), respectively, x_T and x_H are thiophene and n-hexene-1 conversions (%), respectively, $F_{T(H)}$ is the reactant molar flow (mol h^{-1}) and W is the catalyst weight (g);

$$TOF_{HDS}^T = \frac{F_T \cdot x_T \cdot 184}{W \cdot C_{WS_2} \cdot D \cdot 3600} \quad \text{and} \quad TOF_{HYD}^H = \frac{F_H \cdot x_H \cdot 184}{W \cdot C_{WS_2} \cdot D \cdot 3600} , \quad (12)$$

where F_T and F_H are reactant flows (mol h^{-1}); x_T and x_H are conversions (%) of thiophene and n-hexene-1, respectively; W is the catalyst weight (g); C_{WS_2} is the effective WS$_2$ content (wt.%) obtained from XPS, D is the f active phase species dispersion calculated using HRTEM statistics.

To estimate selectivity of the prepared catalysts the HDS/HYDO selectivity factor was calculated [48,54]:

$$\text{Selectivity factor} = \frac{\ln(1 - x_T)}{\ln(1 - x_H)} \quad (13)$$

3. Results and discussion

The chemical composition and textural characteristics of the synthesized (K)-PW/Al$_2$O$_3$ and (K)-Co(Ni)-PW/Al$_2$O$_3$ catalysts are presented in Table 1. The loaded metal amounts (W, Co(Ni) and K) in the samples were close to in value: the tungsten concentration was in the range of 19.5–20.2 wt.%, and cobalt/nickel and potassium amounts were kept constant around 3.1 and 7.5 wt.%, respectively. As the total metal loading was growing, the specific surface area and the total pore volume reduced with the simultaneous maintenance of the average pore diameter. The SSA reduction was not too great (from 173 to 129 m^2/g) and indicated the absence of large crystallites on the carrier surface that were able to block the support pores.

The representative HRTEM micrographs of the prepared (K)-PW/Al$_2$O$_3$ and (K)-Ni(Co)-PW/Al$_2$O$_3$ catalysts are shown in Fig. 1 and the calculated statistics are listed in Table 2. After adding CA to the unpromoted PW catalyst, the dispersion of the active phase species increased due to a decrease of the average linear size of crystallites. The observed phenomenon can be associated with coke species formation from CA molecules during the sulfidation step leading to the partial deposition of coke islands on the most reactive sites of the alumina surface [55]. As a result, the active phase species formed on the coke-free alumina acquired a lower average linear size. Promotion of WS$_2$ crystallites with Co/Ni naturally decreased the average slab length, whereas the modification of the synthesized catalysts with potassium led to the linear crystallite growth, which was probably related to the partial decrease of the interaction between the active phase species and the support. In the K$^+$ excess, a portion of potassium ions could interact with the alumina surface thereby preventing the interaction between the W-based species and the support. The average stacking number was not strongly affected by the Co/Ni addition but the alkali metal-

Table 2
Morphological characteristics of (K)WS$_2$ and (K)-Ni(Co)WS active phase species calculated from HRTEM micrographs of sulfided (K)-PW/Al$_2$O$_3$ and (K)-Ni(Co)-PW/Al$_2$O$_3$ catalysts.

Catalyst	Average length $\bar{L}$ (nm)	Average stacking number $\bar{N}$	Dispersion of (K)WS$_2$ or (K)-Ni(Co)WS particles D^a	$(f_e/f_c)_W$[b]	$(f_e/f_c)_{Co(Ni)W}$[c]
PW/Al$_2$O$_3$	5.8	2.0	0.21	7.6	–
CA-PW/Al$_2$O$_3$	5.1	1.9	0.23	6.5	–
K-PW/Al$_2$O$_3$	7.0	2.0	0.17	9.4	–
Co-PW/Al$_2$O$_3$	4.9	1.9	0.24	6.2	4.0
Ni-PW/Al$_2$O$_3$	4.7	1.9	0.25	5.8	6.1
K-Co-PW/Al$_2$O$_3$	6.3	2.5	0.23	8.3	2.0
K-Ni-PW/Al$_2$O$_3$	6.0	2.3	0.25	7.9	5.6

[a] WS$_2$ dispersion calculated using HRTEM data.
[b] Edge-to-corner ratio of WS$_2$ slab calculated from HRTEM data.
[c] Edge-to-corner ratio of Co(Ni)WS slab calculated from HRTEM and XPS data.
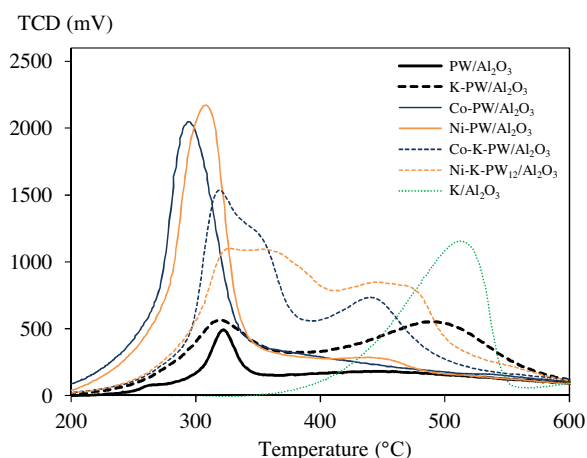
Fig. 2. TPR profiles for sulfided (K)-Ni(Co)-PW/Al$_2$O$_3$ catalysts.

modified catalysts led to a small increase in the amount of slabs in an average Co(Ni)WS$_2$ crystallite. The edge-to-corner ratio of the WS$_2$ slab $(f_e/f_c)_W$ varied widely from 5.8 for the Ni-PW/Al$_2$O$_3$ sample to 9.3 for the K-PW/Al$_2$O$_3$ catalyst, meanwhile the highest edge-to-corner ratio of the promoted slabs was obtained in the Ni-PW/Al$_2$O$_3$ sample.

TPR profiles of sulfided (K)-Ni(Co)-PW/Al$_2$O$_3$ catalysts are shown in Fig. 2. It is known that the first reduction peak corresponds to the edge sulfur reduction [56,57]. PW/Al$_2$O$_3$ catalyst promoting with Co or Ni resulted in the temperature drop at the first reduction peak, meaning that the promoted samples possessed more reactive sites. The peak area also increased indicating the growth in the number of active sites. Further alkali metal modification of the catalysts revealed the opposite effect. There was a rise of the first peak temperature, which implied that the W-S bond strength increased, and the peak area reduction was indicative of the decrease in the content of active sites. The modification of the unpromoted PW/Al$_2$O$_3$ sample with potassium had no effect on the first reduction peak temperature. Consequently, it can be supposed that reactivity of supported WS$_2$ and KWS$_2$ active sites was equal. It also should be noted that the presence of high-temperature peaks (in the range of 441–491 °C) for all K-modified samples was related to the appearance of sulfur atoms with the distinct energy. These peaks could be induced by formation of other active sites with low reactivity. For comparison, the reference K$_2$S/Al$_2$O$_3$ sample reduced at 512 °C. Therefore, high-temperature peaks for the K-modified catalysts could be associated with the K-S bond reduction.

The composition and oxidation state of species on the surface of the sulfided (K)-PW/Al$_2$O$_3$ and (K)-Ni(Co)-PW/Al$_2$O$_3$ catalysts were defined by the XPS analysis. The decomposed W 4f and Co2p/Ni

2p spectra of the synthesized samples are shown in Figs. 3 and 4, respectively. The measured binding energies of all surface species are listed in Table 3. For unmodified Ni(Co)-PW/Al$_2$O$_3$ catalysts, each W 4f spectra consisted of three typical doublets at the following W $4f_{7/2}$ and $4f_{5/2}$ positions: (1) at 32.3 ± 0.1 and 34.3 ± 0.1 eV are associated with W^{4+} in the WS$_2$ phase, (2) at 33.4 ± 0.1 and 35.4 ± 0.1 eV are attributed to W^{5+} in the oxysulfided state, and (3) at 36.0 ± 0.1 and 38.2 ± 0.1 eV are assigned to W^{6+} in the oxygen surrounding. CA had no effect on W species binding energies. All the detected energies were in good agreement with the literature data [22,38,40,43,44,58,59]. For potassium-modified catalysts, the shift around 1.0 eV to the lower binding energies from the initial samples was observed. The indicated shifts can be attributed to partial formation of the octahedral 1T-WS$_2$ phase [60,61]. We had not observed such phenomena for modified K-CoMo systems earlier [51,52], though Cordova et al. reported [62] the detection of 1T-MoS$_2$ phase formation at lower binding energies.

The spectral region of Ni $2p_{3/2}$ and Co $2p_{3/2}$ (Fig. 4) contained three peaks with corresponding satellites. The components at 853.9 and 779.1 eV are associated with Ni in NiWS and Co in CoWS active phases, respectively. The components at 852.8 and 778.6 eV are attributed to Ni and Co in separate sulfides NiS$_x$ and CoS$_x$, respectively. The components at 856.6 and 782.4 eV corresponded to Ni^{2+} and Co^{2+} in the oxygen surroundings, respectively [22,38,40,51,58,59]. The incorporation of potassium had no impact on binding energies of promoter atoms as it had been detected for the W species. For the modified K-Co(Ni)-PW/Al$_2$O$_3$ samples in the W 4f region, the contribution of K 3s at about 33.5 ± 0.1 eV and K $2p_{3/2}$ at 292.8 ± 0.1 was also detected corresponding to the K$^+$ state [63]. There were no potassium sulfates observed in the XPS spectra.

The decomposition of the recorded spectra allowed calculating the distribution for nickel (cobalt) and tungsten species present on the surface of the sulfided (K)-PW/Al$_2$O$_3$ and (K)-Co(Ni)-PW/Al$_2$O$_3$ catalysts. Modifying of the synthesized catalysts with the alkali metal led to the strong decrease in the amount of CoWS and NiWS active phases from 43 to 8% rel. and from 48 to 29% rel., respectively. Simultaneous CoS$_x$ and NiS$_x$ buildups from 49 to 81% rel. and from 31 to 60% rel., respectively, were also observed. Using of CA in catalyst preparation led to a slight increase of the W sulfidation degree with the decrease in the amount of oxysulfides and W in the oxygen surroundings as well, what also evidenced to diminishing of the interaction between the active metal and the support caused by the chelating agent. Promoting of the PW/Al$_2$O$_3$ catalyst with Co had no effect on the WS$_2$ amount, though the WS$_x$O$_y$ content was distinctly higher and the W^{6+} amount, on the contrary, was lower. Further modifying of the Co-PW/Al$_2$O$_3$ sample with potassium amplified the transformation of W^{6+} to W^{5+} components even more. For the Ni-containing samples, we observed the W sulfidation degree reduction with the increasing the amount of oxysulfides both in the promoted sample and in the K-modified one in
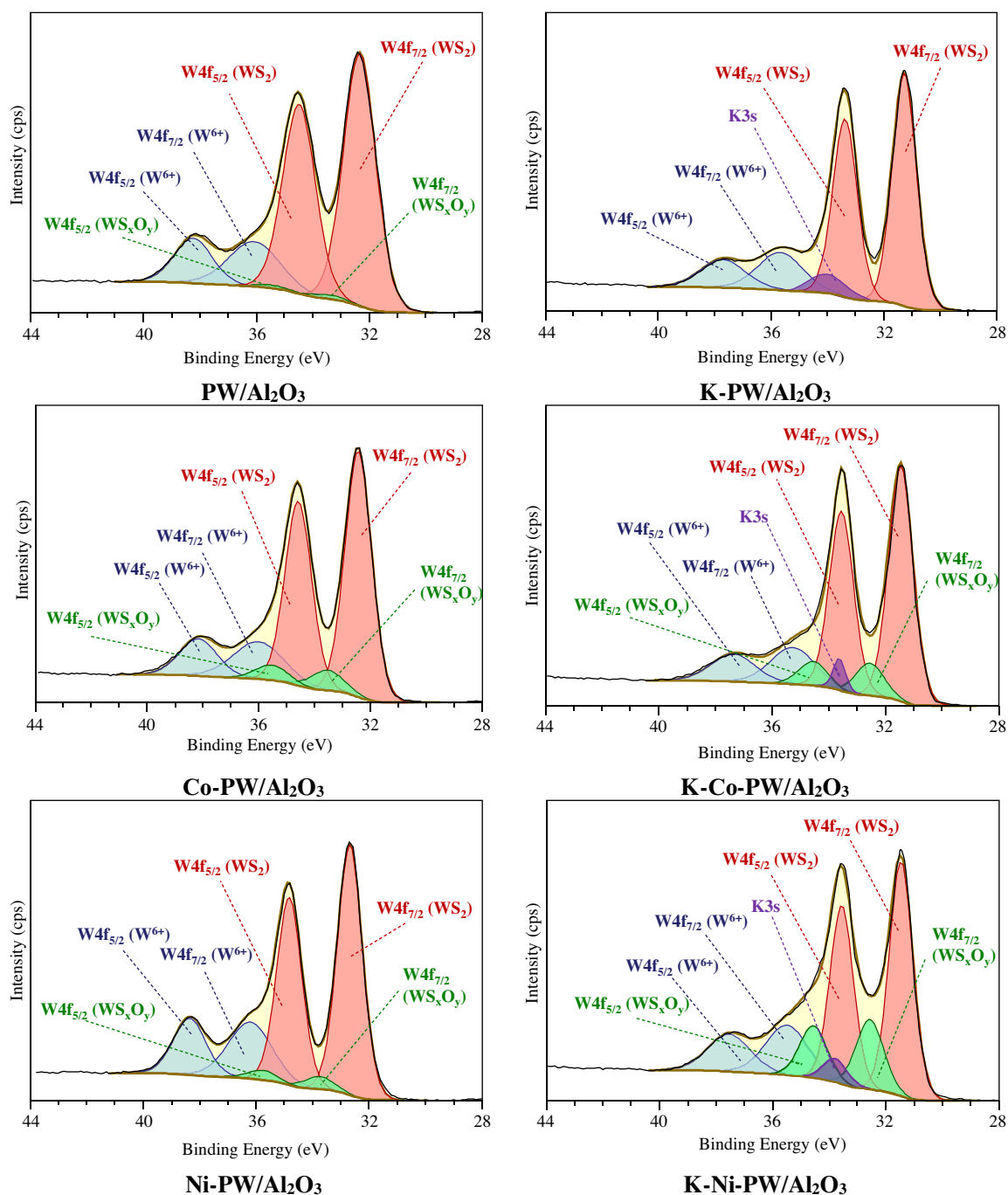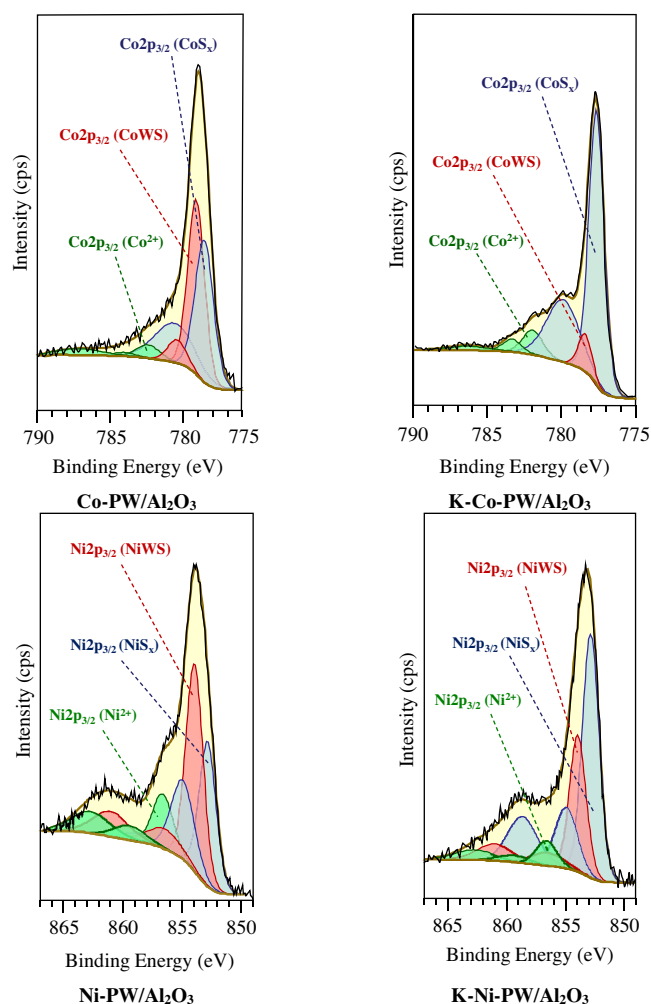
Fig. 3. XPS W 4f spectra recorded for (K)-PW/Al$_2$O$_3$ and (K)-Ni(Co)-PW/Al$_2$O$_3$ catalysts; in blue: W^{6+} oxide contributions; in green: WS$_x$O$_y$ contributions; in red: WS$_2$ contributions (For interpretation of the references to color in this figure legend, the reader is referred to the web version of the article.).

Table 3
Binding energies (eV) measured by XPS for cobalt, nickel, tungsten, and sulfur species present on the surface of sulfided (K)-PW/Al$_2$O$_3$ and (K)-Ni(Co)-PW/Al$_2$O$_3$ catalysts.

Catalyst	Co 2$p_{3/2}$			Ni 2$p_{3/2}$			W4$f_{7/2}$			S 2$p_{3/2}$ S^{2-}
	CoWS	CoS$_x$	Co^{2+}	NiWS	NiS$_x$	Ni^{2+}	WS$_2$	WS$_x$O$_y$	W^{6+}	
PW/Al$_2$O$_3$	–	–	–	–	–	–	32.3	33.4	36.1	161.9
CA-PW/Al$_2$O$_3$	–	–	–	–	–	–	32.3	33.4	36.1	161.9
K-PW/Al$_2$O$_3$	–	–	–	–	–	–	31.3	32.4	35.7	160.8
Co-PW/Al$_2$O$_3$	779.1	778.6	782.4	–	–	–	32.4	33.5	36.0	162.0
Ni-PW/Al$_2$O$_3$	–	–	–	853.9	852.8	856.6	32.4	33.7	35.9	162.2
K-Co-PW/Al$_2$O$_3$	778.8	778.3	782.2	–	–	–	31.5	32.6	35.3	161.2
K-Ni-PW/Al$_2$O$_3$	–	–	–	853.9	852.8	856.6	31.5	32.6	35.5	161.1

Fig. 4. XPS Co 2p and Ni 2p spectra recorded for (K)-Ni(Co)-PW/Al$_2$O$_3$ catalysts; in blue: Co^{2+} (Ni^{2+}) oxide contributions; in green: CoS$_x$ (NiS$_x$) contributions; in red: CoWS (NiWS) phase contributions (For interpretation of the references to color in this figure legend, the reader is referred to the web version of the article.).

comparison with the CoPW/Al$_2$O$_3$ catalyst. Moreover, alkali metal-modifying of the promoted W-based catalysts led to a decrease of the edge promotion ratio for both Ni- and Co-promoted samples.

The catalytic properties of the prepared (K)-PW/Al$_2$O$_3$ and (K)-Co(Ni)-PW/Al$_2$O$_3$ catalysts in HDT of the model feed are listed in Table 5. The K-modification of samples, whether promoted or unpromoted, impacted catalyst activities equally: both HDS and HYDO conversions went down. For the (K)-PW/Al$_2$O$_3$ samples, the activity loss was around 89 rel.% in the thiophene conversion (rate constants decreased from 1.4×10^{-5} to 0.2×10^{-5} mol h^{-1} g^{-1}) and around 99.5 rel.% in the n-hexene-1 conversion (rate constants decreased from 512×10^{-5} to 2×10^{-5} mol h^{-1} g^{-1}). A similar effect was observed for the (K)-Co(Ni)-PW/Al$_2$O$_3$ formulations. The loss in HDS and HYDO activities with the Co-promoted systems was about 57 rel.% (rate constants decreased from 3.2×10^{-5} to 1.2×10^{-5} mol h^{-1} g^{-}) and 32 rel.% (rate constants decreased from 28×10^{-5} to 19×10^{-5} mol h^{-1} g^{-1}), respectively. The greatest loss in activity was detected for the Ni-promoted systems. For unmodified system, HDS and HYDO rate constants appeared at the level of 98.9×10^{-5} and 6995×10^{-5} mol h^{-1} g^{-1}, respectively. After potassium loading, HDS and HYDO rate constants decreased to the level of 0.5×10^{-5} and 126×10^{-5} mol h^{-1} g^{-1}. It should be noticed that the unmodified Ni-PW/Al$_2$O$_3$ catalyst possessed the highest activity in HDT of the model feed, whereas after the modification

Table 4
Metal distribution for cobalt (nickel) and tungsten species present on the surface of sulfided (K)-PW/Al$_2$O$_3$ and (K)-Ni(Co)-PW/Al$_2$O$_3$ catalysts.

Catalyst	(Co/W)$_{tot}$/(Ni/W)$_{tot}$ [a]	(Co/W)$_{slab}$/(Ni/W)$_{slab}$ [b]	(Co/W)$_{edge}$/(Ni/W)$_{edge}$ [c]	Number of W^{IV} edge sites (10^{20} at g^{-1})	Co distribution (rel.%)			Ni distribution (rel.%)			W distribution (rel.%)		
					CoWS	CoS$_x$	Co^{2+}	NiWS	NiS$_x$	Ni^{2+}	WS$_2$	WS$_x$O$_y$	W^{6+}
PW/Al$_2$O$_3$	–	–	–	0.9	–	–	–	–	–	–	69	3	28
CA-PW/Al$_2$O$_3$	–	–	–	0.8	–	–	–	–	–	–	72	1	27
K-PW/Al$_2$O$_3$	–	–	–	0.6	–	–	–	–	–	–	71	1	28
Co-PW/Al$_2$O$_3$	0.26	0.16	0.64	0.8	43	49	8	–	–	–	70	9	21
Ni-PW/Al$_2$O$_3$	0.34	0.25	0.98	1.1	–	–	–	48	31	21	66	6	28
K-Co-PW/Al$_2$O$_3$	0.38	0.05	0.24	0.6	8	81	10	–	–	–	69	12	19
K-Ni-PW/Al$_2$O$_3$	0.32	0.15	0.75	0.6	–	–	–	29	60	11	61	18	21

[a] Co/W or Ni/W total atomic ratio calculated from XPS results.
[b] Co/W or Ni/W ratio in CoWS slabs calculated from XPS results.
[c] Co/W or Ni/W ratio in CoWS edges calculated from XPS and HRTEM results.

with the alkali metal, the activity level became the lowest. Similar dependences were observed for TOF values of the Co-promoted catalysts. Adding of CA to the unpromoted W-based sample led to the double growth of the HDS TOF number and to the 2.3 times increase in the HYDO TOF number, what indicated the rise of reactivity of both active site types. As a result, the HDS/HYDO selectivity factor slightly decreased. After the potassium incorporation to the PW/Al$_2$O$_3$ catalyst, the values of both the HDS and the HYDO TOF number dropped drastically to 70 and 99 rel.%, respectively. Hence, the HDS/HYDO selectivity rose by far.

For the Co-promoted sample, we observed the 4-fold increase of HDS and the 1.6-fold increase of HYDO TOF values compared to the unpromoted PW/Al$_2$O$_3$ catalyst. In the Ni-promoted sample, both the HDS and the HYDO TOF number showed a great growth—62 times and 22 times, respectively. Therefore, the promotion of catalysts with Co/Ni led to the rise in reactivity of the active site edges. Also, the TPR analysis indicated by where the first reduction peak at the TPR curves had shifted towards lower temperatures (Fig. 2). In addition, the NiW catalyst appeared far more active than the CoW sample for HDT of model FCC gasoline, which is in good agreement with previously reported data [21,22]. The potassium-modification of either Co- or Ni-promoted catalysts revealed the opposite effect. Despite that, the potassium addition decreased both the HDS and the HYDO TOF number, HDS was more sensitive to the modification than HYDO. With the K-Co-PW/Al$_2$O$_3$ catalyst, TOF numbers for HDS and HYDO reactions decreased to 45 and 11 rel.%, respectively. For the K-Ni-PW/Al$_2$O$_3$ sample, such reductions were much more pronounced and achieved 98 and 95 rel.%. The obtained data were also in consistency with the TPR results: the decrease of the TOF values due to alkali metal-modifying was accompanied by the first reduction peak shift towards high temperatures (Fig. 2).

It is interesting to note that the Ni-promoted sample proved to be more sensitive to the potassium addition than the Co-promoted one. Moreover, it is worth to remind that potassium favored the migration of promoter atoms from the active phase to separate sulfides (Table 4); it was especially vivid in the Co-promoted sample. In fact, active components of the K-Co-PW/Al$_2$O$_3$ catalysts were present as a mixture of CoS$_x$ and KWS species. The promoter migration was also detected in the K-Ni-PW/Al$_2$O$_3$ sample though not to such a high extent. Therefore, the active phase of Ni-promoted modified catalysts is likely to be the KNiWS species. The distinction in the promoters' behavior during the catalyst modification can be associated with their localization on the edges of WS$_2$ crystallites. It is assumed that Co atoms preferably fix on the S-edge of Mo(W)S$_2$, whereas Ni atoms can decorate both M- and S-edges [64,65]. Probably, the potassium incorporation favored the lowering of the bonding energy of the promoter with atoms on the edge. Since the fixation of Ni atoms on the WS$_2$ edge was stronger than that of Co atoms, Co atoms migrated from the active phase to a greater degree. Eventually, the modified catalysts can be ranged by activity as follows: KWS < KNiWS « CoS$_x$ + KWS. It is interesting that the CoS$_x$ + KWS mixture appeared the most active, though the relative amount of the CoWS active phase in such catalyst, as shown by the XPS analysis, was less than in the K-Ni-PW/Al$_2$O$_3$ sample. It could be caused by the contribution of the spillover effect from CoS$_x$ species, which are famous for the hydrogen activation with a subsequent rise of Mo(W)S$_2$ activity [66,67].

Another curious observation was that only in the instance of the unpromoted PW/Al$_2$O$_3$ catalyst the modification with the alkali metal led to the growth of the HDS/HYDO selectivity factor. It differed from CoMo systems where the potassium modification resulted in the significant increase of HDS/HYDO selectivity [51]. While studying CoMo systems with various morphological characteristics of the active phase and K-modified CoMo systems, it was found that the HDS/HYDO selectivity factor increased with the rise of the edge-to-corner ratio of CoMoS slabs [51,52,54], although
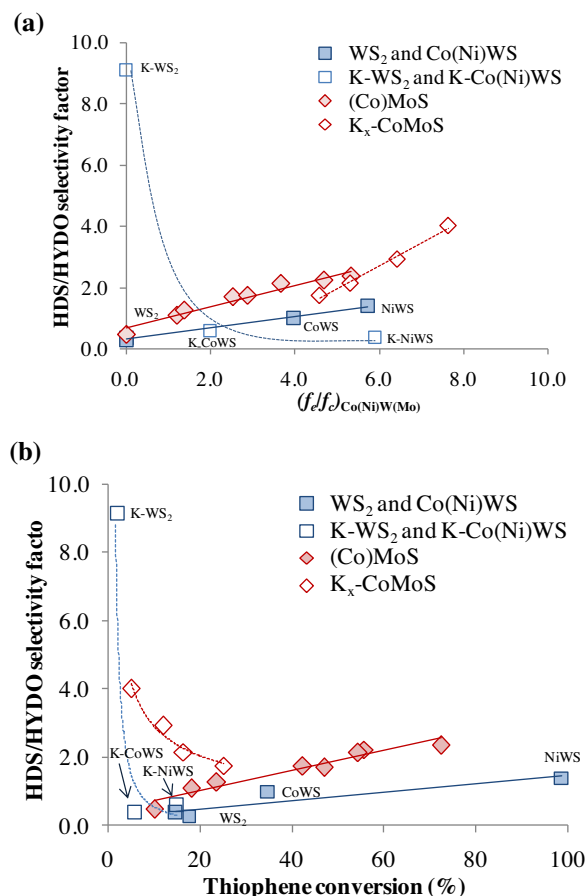

Fig. 5. Dependence of the HDS/HYDO selectivity factor in HDT of a mixture of thiophene and *n*-hexene-1 from the ratio of the number of edge's to corner's Co(Ni) atoms (a) and the HDS conversion (b) for Co-PMo/Al$_2$O$_3$ [54], K$_x$-Co-PMo/Al$_2$O$_3$ [51], (K)-PW/Al$_2$O$_3$, and (K)-Ni(Co)-PW/Al$_2$O$_3$ catalysts.

the dependence of HDS/HYDO selectivity from the edge-to-corner ratio of CoMoS slabs for modified catalysts was more drastic than for unmodified ones. That was assumed as the evidence of active site nature changing by the potassium addition. To better understand the relationship between the ratio of the number of edge's to corner's Co(Ni) atoms and HDS/HYDO selectivity of the unmodified and K-modified Ni(Co)W catalysts, the corresponding dependences were plotted (Fig. 5a). The observed tendency for the unmodified catalysts was the same as for the Mo-based systems: the increase in the edge-to-corner ratio of Co(Ni)WS slabs induced the rise in HDS/HYDO selectivity, though the resulting Co(Ni)W species selectivity was lower for the same values of the edge-to-corner ratio of Co(Ni)W(Mo)S slabs. Modifying of the non-promoted W-based system greatly increased the HDS/HYDO selectivity factor, whereas the opposite phenomenon was observed for the Co- or Ni-promoted samples—HDS/HYDO selectivity fell down. Therefore, the potassium incorporation poisoned active sites both of the W-based catalysts and of the Mo-based ones, yet the morphological effect was not the same as we had observed earlier [51]—the sulfidation degree of active metals decreased and the linear size of active phase crystallites did not grow much. As a result, the HDS/HYDO selectivity factor dropped after the modification.

Another interesting finding was the dependence of the HDS/HYDO selectivity factor from the thiophene conversion in all groups of the tested catalysts (Fig. 5b). For the unmodified samples, the selectivity growth was followed by the HDS activity increase, although the HDS/HYDO selectivity factor values were not high. The potassium addition led to a reversal of the dependence: the

Table 5
Catalytic properties of prepared (K)-PW/Al$_2$O$_3$ and (K)-Ni(Co)-PW/Al$_2$O$_3$ catalysts in HDT of a mixture of thiophene and n-hexene-1 (T = 250 °C, P = 1.5 MPa, LHVS = 5 h^{-1}, H$_2$/feed = 100 nL/L).

Catalyst	Conversion (%)		Rate constant × 10^5 (mol h^{-1} g^{-1})		TOF values (× 10^{-4} s^{-1})		Selectivity factor HDS/HYD
	Thiophene	Hexene-1	k_{HDS}	k_{HYD}	Thiophene HDS	Hexene-1 HYD	
PW/Al$_2$O$_3$	15	29	1.2	334	0.20	50	0.4
CA-PW/Al$_2$O$_3$	18	41	1.4	512	0.26	79	0.3
K-PW/Al$_2$O$_3$	2.0	0.2	0.2	2	0.04	0.4	9.1
Co-PW/Al$_2$O$_3$	35	28	3.2	319	0.53	55	1.0
Ni-PW/Al$_2$O$_3$	73[a]	51[a]	98.9	6995	8.1	738	1.4
K-Co-PW/Al$_2$O$_3$	15	19	1.2	212	0.29	49	0.7
K-Ni-PW/Al$_2$O$_3$	5.9	12.1	0.5	126	0.13	34	0.4

[a] LHVS = 50 h^{-1}.

higher the HDS/HYDO selectivity factor the lower the thiophene conversion. Consequently, high HDS/HYDO selectivity is only possible with a simultaneous decrease of the HDS conversion. Thus, designing of a catalyst for selective HDT of specified FCC gasoline needs striking a balance between the required HDS/HYDO selectivity factor and a reasonable HDS degree. Ni-WS/Al$_2$O$_3$ catalysts with high HDS activity and satisfactory HDS/HYDO selectivity are of choice for feeds with a high sulfur concentration. K-modified CoMo systems are preferable for low sulfur feeds with a great amount of olefins.

4. Conclusions

The incorporation of potassium influenced both the catalyst active phase characteristics and catalytic properties of the (K)-Ni(Co)-PW/Al$_2$O$_3$ samples. The alkali modifier induced: (i) small growth of the average slab length of crystallites; (ii) decrease of reactivity and the number of active sites of the K-Ni(Co)-PW/Al$_2$O$_3$ catalysts that appeared in shifting of the first TPR peaks towards higher temperatures; (iii) feasible partial formation of the octahedral 1T-WS$_2$ phase that followed due to the shift around 1.0 eV to lower binding energies from the initial samples; (iv) strong decrease in the amount of CoWS and NiWS active phases in parallel with growth of CoS$_x$ and NiS$_x$ species; (v) drastic drop of HDS and HYD activities with the HDS/HYDO selectivity decrease in the Ni- and Co-promoted systems and with the great rise of the selectivity factor in the case of the K-unpromoted catalyst.

The Ni-promoted catalyst proved to be more sensitive to the K-modification than the Co-promoted sample. In fact, the potassium incorporation into the active phase of the K-Co-PW/Al$_2$O$_3$ catalyst resulted in a mixture of CoS$_x$ and KWS species due to the partial migration of Co atoms, whereas, in the case of the K-Ni-PW/Al$_2$O$_3$ catalyst, the active phase can assumingly be the KNiWS species. Hence, the modified catalysts can be ranged by the activity level as follows: KWS < KNiWS « CoS$_x$ + KWS.

The balance between HDS/HYDO selectivity and HDS activity appears a key factor for developing a catalyst for selective HDT of FCC gasoline. The main factor for selecting a catalyst is the FCC gasoline composition: NiWS systems with high HDS activity and satisfactory HDS/HYDO selectivity are preferable for high sulfur feeds whereas KCoMoS formulations are of choice for low sulfur gasolines with a great amount of olefins.

Acknowledgments

References

[1] S. Brunet, D. Mey, G. Perot, C. Bouchy, F. Diehl, On the hydrodesulfurization of FCC gasoline: a review, Appl. Catal. A 278 (2005) 143–172.
[2] M. Breysse, G. Djega-Mariadassou, S. Pessayre, C. Geantet, M. Vrinat, G. Pérot, M. Lemaire, Deep desulfurization: reactions, catalysts and technological challenges, Catal. Today 84 (2003) 129–138.
[3] A. Duan, R. Li, G. Jianga, J. Gao, Z. Zhao, G. Wan, D. Zhang, W. Huang, K.H. Chung, Hydrodesulphurization performance of NiW/TiO$_2$-Al$_2$O$_3$ catalyst for ultra clean diesel, Catal. Today 140 (2009) 187–191.
[4] X. Tao, Y. Zhou, Q. Wei, Q. Cui, J. Liu, T. Liu, Effect of morphology properties of NiW catalysts on hydrodesulfurization for individual sulfur compounds in fluid catalytic cracking diesel, Fuel Process. Technol. 118 (2014) 200–207.
[5] G. Wan, A. Duan, Y. Zhang, Z. Zhao, G. Jiang, D. Zhang, J. Liu, K. Chung, NiW/AMBT catalysts for the production of ultra-low sulfur diesel, Catal. Today 158 (2010) 521–529.
[6] P.E. Boahene, K.K. Soni, A.K. Dalai, J. Adjaye, Hydroprocessing of heavy gas oils using FeW/SBA-15 catalysts: experimentals, optimization of metals loading, and kinetics study, Catal. Today 207 (2013) 101–111.
[7] R.A. Diaz-Real, R.S. Mann, I.S. Sambi, Hydrotreatment of Athabasca bitumen derived gas oil over nickel-molybdenum nickel-tungsten, and cobalt-molybdenum catalysts, Ind. Eng. Chem. Res. 32 (1993) 1354–1358.
[8] R. Sahu, B.J. Song, J.S. Im, Y.-P. Jeon, C.W. Lee, A review of recent advances in catalytic hydrocracking of heavy residues, J. Ind. Eng. Chem. 27 (2015) 12–24.
[9] Y.G. Hur, M.-S. Kim, D.-W. Lee, S. Kim, H.-J. Eom, G. Jeong, M.-H. No, N.S. Nho, K.-Y. Lee, Hydrocracking of vacuum residue into lighter fuel oils using nanosheet-structured WS$_2$ catalyst, Fuel 137 (2014) 237–244.
[10] M. Absi-Halabi, A. Stanislaus, K. Al-Dolama, Performance comparison of alumina-supported Ni-Mo, Ni-W and Ni-Mo-W catalysis in hydrotreating vacuum residue, Fuel 77 (1998) 787–790.
[11] C. Komintarachat, S. Chuepeng, Solid acid catalyst for bio diesel production from waste used cooking oils, Ind. Eng. Chem. Res. 48 (2009) 9350–9353.
[12] K. Srilatha, T. Issariyakul, N. Lingaiah, P.S. Sai Prasad, J. Kozinski, A.K. Dalai, Efficient esterification and transesterification of used cooking oil using 12-tungstophosphoric acid (TPA)/Nb$_2$O$_5$ catalyst, Energy Fuels 24 (2010) 4748–4755.
[13] S. Ramu, N. Lingaiah, B.L.A. Prabhavathi Devi, R.B.N. Prasad, I. Suryanarayana, P.S.S. Prasad, Esterification of palmitic acid with methanol over tungsten oxide supported on zirconia solid acid catalysts: effect of method of preparation of the catalyst on its structural stability and reactivity, Appl. Catal. A 276 (2004) 163–168.
[14] M.G. Kulkarni, R. Gopinath, L.C. Mehera, A.K. Dalai, Solid acid catalyzed biodiesel production by simultaneous esterification and transesterification, Green Chem. 8 (2006) 1056–1062.
[15] A.E.C. Barrón, J.A. Melo-Banda, J.M.E. Dominguez, E.M. Hernández, R.R. Silva, A.I.T. Reyes, M.A.M. Meraz, Catalytic hydrocracking of vegetable oil for agrofuels production using Ni-Mo, Ni-W, Pt and TFA catalysts supported on SBA-15, Catal. Today 166 (2011) 102–110.
[16] Ch. Kordulis, A.A. Lappas, Ch. Fountzoula, K. Drakaki, A. Lycourghiotis, I.A. Vasalos, W/γ-Al$_2$O$_3$ catalysts prepared by modified equilibrium deposition filtration (MEDF) and non-dry impregnation (NDI): Characterization and catalytic activity evaluation for the production of low sulfur gasoline in a HDS pilot plant, Appl. Catal. A 209 (2001) 85–95.
[17] Sh. Shan, P. Yuan, W. Han, G. Shi, X. Bao, Supported NiW catalysts with tunable size and morphology of active phases for highly selective hydrodesulfurization of fluid catalytic cracking naphtha, J. Catal. 330 (2015) 288–301.
[18] Y. van der Meer, M.J. Vissenberg, V.H.J. de Beer, J.A.R. van Veen, A.M. van der Kraan, Characterization of carbon- and alumina-supported NiW and CoW sulfided catalysts, Ind. Appl. Mössbauer Effect Springer 45 (2002) 51–57.
[19] M. Brorson, A. Carlsson, H. Topsøe, The morphology of MoS$_2$, WS$_2$, Co-Mo-S, Ni-Mo-S and Ni-W-S nanoclusters in hydrodesulfurization catalysts revealed by HAADF-STEM, Catal. Today 123 (2007) 31–36.

[20] A. Carlsson, M. Brorson, H. Topsøe, Morphology of WS_2 nanoclusters in WS_2/C hydrodesulfurization catalysts revealed by high-angle annular dark field scanning transmission electron microscopy (HAADF-STEM) imaging, J. Catal. 227 (2004) 530–536.

[21] J. Espino, L. Alvarez, C. Ornelas, J.L. Rico, S. Fuentes, G. Berhault, G. Alonso, Comparative study of WS_2 and Co (Ni)/WS_2 HDS catalysts prepared by ex situ/in situ activation of ammonium thiotungstate, Catal. Lett. 90 (2003) 71–80.

[22] L. Coulier, G. Kishan, J.A.R. van Veen, J.W. Niemantsverdriet, Influence of support-interaction on the sulfidation behavior and hydrodesulfurization activity of Al_2O_3-supported W, CoW, and NiW model catalysts, J. Phys. Chem. B. 106 (2002) 5897–5906.

[23] J.G. Speight, The Chemistry and Technology of Petroleum, fourth ed., Taylor & Francis, Boca Raton, Fla, 2007.

[24] E.J.M. Hensen, Y. van der Meer, J.A.R. van Veen, J.W. Niemantsverdriet, Insight into the formation of the active phases in supported NiW hydrotreating catalysts, Appl. Catal. A 322 (2007) 16–32.

[25] A. Spojakina, R. Palcheva, K. Jiratova, G. Tyuliev, L. Petrov, Synergism between Ni and W in the NiW/γ-Al_2O_3 hydrotreating catalysts, Catal. Lett. 104 (2005) 45–52.

[26] Y. Ji, P. Afanasiev, M. Vrinat, W. Li, C. Li, Promoting effects in hydrogenation and hydrodesulfurization reactions on the zirconia and titania supported catalysts, Appl. Catal. A 257 (2004) 157–164.

[27] G.M. Dhar, B.N. Srinivas, M.S. Rana, M. Kumar, S.K. Maity, Mixed oxide supported hydrodesulfurization catalysts a review, Catal. Today 86 (2003) 45–60.

[28] P. Gheek, S. Suppan, J. Trawczyński, A. Hynaux, C. Sayag, G. Djega-Mariadssou, Carbon black composites-supports of HDS catalysts, Catal. Today 119 (2007) 19–22.

[29] J.N.D. de León, V. Petranovskii, J.A. de los Reyes, G. Alonso-Nuñez, T.A. Zepeda, S. Fuentes, J.L. García-Fierro, One dimensional (1D) γ-alumina nanorod linked networks: synthesis, characterization and application, Appl. Catal. A 472 (2014) 1–10.

[30] H. Li, M. Li, Ya. Chu, F. Liu, H. Nie, Essential role of citric acid in preparation of efficient NiW/Al_2O_3 HDS catalysts, Appl. Catal. A 403 (2011) 75–82.

[31] G. Kishan, L. Coulier, V.H.J. de Beer, J.A.R. van Veen, J.W. Niemantsverdriet, Sulfidation and thiophene hydrodesulfurization activity of nickel tungsten sulfide model catalysts, prepared without and with chelating agents, J. Catal. 196 (2000) 180–189.

[32] Y. Ohta, T. Shimizu, T. Honma, M. Yamada, Effect of chelating agents on HDS and aromatic hydrogenation over CoMo-and NiW/Al_2O_3, Stud. Surf. Sci. Catal. 127 (1999) 161–168.

[33] T. Shimizu, K. Hiroshima, T. Honma, T. Mochizuki, M. Yamada, Highly active hydrotreatment catalysts prepared with chelating agents, Catal. Today 45 (1998) 271–276.

[34] C.E. Santolalla-Vargas, V.A. Suarez Toriello, J.A. de los Reyes, D.K. Cromwell, B. Pawelec, J.L.G. Fierro, Effects of pH and chelating agent on the NiWS phase formation in NiW/γ-Al_2O_3 HDS catalysts, Mater. Chem. Phys. 166 (2015) 105–115.

[35] V.A. Suárez-Toriello, C.E. Santolalla-Vargas, J.A. de losReyesa, A. Vázquez-Zavala, M. Vrinat, C. Geantet, Influence of the solution pH in impregnation with citric acid and activity of Ni/W/Al_2O_3 catalysts, J. Mol. Catal. A: Chem. 404 (2015) 36–46.

[36] R. Palcheva, A. Spojakina, G. Tyuliev, K. Jiratova, L. Petrov, The effect of nickel on the component state and HDS activity of alumina-supported heteropolytungstates, Kinet. Catal. 48 (2007) 847–852.

[37] R. Shafi, M.R.H. Siddiqui, G.J. Hutchings, E.G. Derouane, I.V. Kozhevnikov, Heteropoly acid precursor to a catalyst for dibenzothiophene hydrodesulfurization, Appl. Catal. A 204 (2000) 251–256.

[38] K.B. Tayeb, C. Lamonier, C. Lancelot, M. Fournier, A. Bonduelle-Skrzypczak, F. Bertoncini, Increase of the Ni/W ratio in heteropolyanions based NiW hydrocracking catalysts with improved catalytic performances, Catal. Lett. 144 (2014) 460–468.

[39] C. Larabi, W. al Maksoud, K.C. Szeto, A. Roubaud, P. Castelli, C.C. Santini, J.J. Walter, Thermal decomposition of lignocellulosic biomass in the presence of acid catalysts, Bioresour. Technol. 148 (2013) 255–260.

[40] K.B. Tayeb, C. Lamonier, C. Lancelot, M. Fournier, E. Payen, A. Bonduelle, F. Bertoncini, Study of the active phase of NiW hydrocracking sulfided catalysts obtained from an innovative heteropolyanion based preparation, Catal. Today 150 (2010) 207–212.

[41] R. Palcheva, A. Spojakina, L. Dimitrov, K. Jiratova, 12-Tungstophosphoric heteropolyacid supported on modified SBA-15 as catalyst in HDS of thiophene, Microporous Mesoporous Mater. 122 (1–3) (2009) 128–134.

[42] K.B. Tayeb, C. Lamonier, C. Lancelot, M. Fournier, A. Bonduelle-Skrzypczak, F. Bertoncini, Active phase genesis of NiW hydrocracking catalysts based on nickel salt heteropolytungstate: comparison with reference catalyst, Appl. Catal. B 126 (2012) 55–63.

[43] P.P. Minaev, P.A. Nikulshin, M.S. Kulikova, A.A. Pimerzin, V.M. Kogan, NiWS/Al_2O_3 hydrotreating catalysts prepared with 12-tungstophosphoric heteropolyacid and nickel citrate: effect of Ni/W ratio, Appl. Catal. A 505 (2015) 456–466.

[44] P.A. Nikulshin, P.P. Minaev, A.V. Mozhaev, K.I. Maslakov, M.S. Kulikova, A.A. Pimerzin, Investigation of co-effect of 12-tungstophosphoric heteropolyacid, nickel citrate and carbon-coated alumina in preparation of NiW catalysts for HDS, HYD and HDN reactions, Appl. Catal. B 176 (2015) 374–384.

[45] P. Nikulshin, A. Mozhaev, C. Lancelot, P. Blanchard, E. Payen, C. Lamonier, Hydroprocessing catalysts based on transition metal sulfides prepared from Anderson and dimeric Co_2Mo_{10}-heteropolyanions. A review, C.R. Chimie 19 (2016) 1276–1285.

[46] T. Alphazan, A. Bonduelle-Skrzypczak, C. Legens, Z. Boudene, A.-L. Taleb, A.-S. Gay, O. Ersen, C. Copéret, P. Raybaud, Improved promoter effect in NiWS catalysts through a molecular approach and an optimized Ni edge decoration, J. Catal. 340 (2016) 60–65.

[47] H. Wang, Z. Yao, X. Zhan, Y. Wua, M. Li, Preparation of highly dispersed W/ZrO_2-Al_2O_3 hydrodesulfurization catalysts at high WO_3 loading via a microwave hydrothermal method, Fuel 158 (2015) 918–926.

[48] T. Kabe, Y. Aoyama, D. Wang, A. Ishihara, W. Qian, M. Hosoya, Q. Zhang, Effects of H_2S on hydrodesulfurization of dibenzothiophene and 4,6-dimethyldibenzothiophene on alumina-supported NiMo and NiW catalysts, Appl. Catal. A 209 (2001) 237–247.

[49] W.R.A.M. Robinson, J.A.R. van Veen, V.H.J. de Beer, R.A. van Santen, Development of deep hydrodesulfurization catalysts: II. NiW, Pt and Pd catalysts tested with (substituted) dibenzothiophene, Fuel Process. Technol. 61 (1999) 103–116.

[50] H.R. Reinhoudt, R. Troost, A.D. van Langeveld, S.T. Sie, J.A.R. van Veen, J.A. Moulijn, Catalysts for second-stage deep hydrodesulfurisation of gas oils, Fuel Process. Technol. 61 (1999) 133–147.

[51] D. Ishutenko, P. Nikulshin, A. Pimerzin, Relation between composition and morphology of K(Co)MoS active phase species and their performances in hydrotreating of model FCC gasoline, Catal. Today 271 (2016) 16–27.

[52] P. Nikulshin, D. Ishutenko, Yu. Anashkin, A. Mozhaev, A. Pimerzin, Selective hydrotreating of FCC gasoline over KCoMoP/Al_2O_3 catalysts prepared with $H_3PMo_{12}O_{40}$: Effect of metal loading, Fuel 182 (2016) 632–639.

[53] S. Kasztelan, H. Toulhoat, J. Grimblot, J.P. Bonnelle, A geometrical model of the active phase of hydrotreating catalysts, Appl. Catal. 13 (1984) 127–159.

[54] P.A. Nikulshin, D.I. Ishutenko, A.A. Mozhaev, K.I. Maslakov, A.A. Pimerzin, Effects of composition and morphology of active phase of CoMo/Al_2O_3 catalysts prepared using Co_2Mo_{10}-heteropolyacid and chelating agents on their catalytic properties in HDS and HYD reactions, J. Catal. 312 (2014) 152–169.

[55] P.A. Nikulshin, V.A. Salnikov, A.V. Mozhaev, P.P. Minaev, V.M. Kogan, A.A. Pimerzin, Relationship between active phase morphology and catalytic properties of the carbon-alumina-supported Co(Ni)Mo catalysts in HDS and HYD reactions, J. Catal. 309 (2014) 386–396.

[56] B. Scheffer, N.J.J. Dekker, P.J. Mangnus, J.A. Moulijn, A temperature-programmed reduction study of sulfide Co-Mo/Al_2O_3 hydrodesulfurization catalysts, J. Catal. 121 (1990) 31–46.

[57] J.B. McGarvey, S. Kasztelan, An investigation on the reduction behavior of MoS_2/Al_2O_3 and the subsequent detection of hydrogen on the surface, J. Catal. 148 (1994) 149–156.

[58] D. Zuo, M. Vrinat, H. Nie, F. Maugé, Y. Shi, M. Lacroix, D. Li, The formation of the active phases in sulfide NiW/Al_2O_3 catalysts and their evolution during post-reduction treatment, Catal. Today 93–95 (2004) 751–760.

[59] J.C. Mogica-Betancourt, A. López-Benítez, J.R. Montiel-López, L. Massin, M. Aouine, M. Vrinat, G. Berhault, A. Guevara-Lara, Interaction effects of nickel polyoxotungstate with the Al_2O_3-MgO support for application in dibenzothiophenehydrodesulfurization, J. Catal. 313 (2014) 9–23.

[60] D. Voiry, H. Yamaguchi, J. Li, R. Silva, D. Alves, T. Fujita, M. Chen, T. Asefa, V. Shenoy, G. Eda, M. Chhowalla, Enhanced catalytic activity in strained chemically exfoliated WS_2 nanosheets for hydrogen evolution, Nat. Mater. 12 (2013) 850–855.

[61] B. Mahler, V. Hoepfner, K. Liao, G.A. Ozin, Colloidal synthesis of 1T-WS_2 and 2H-WS_2 nanosheets: applications for photocatalytic hydrogen evolution, J. Am. Chem. Soc. 136 (2014) 14121–14127.

[62] A. Cordova, P. Blanchard, C. Lancelot, G. Fremy, C. Lamonier, Probing the nature of the active phase of molybdenum-supported catalysts for the direct synthesis of methylmercaptan from syngas and H_2S, ACS Catal. 5 (2015) 2966–2981.

[63] S. Bruyère, B. Domenichini, V. Potin, Z. Li, S. Bourgeois, WO_x phase growth on SiO_2/Si by decomposition of tungsten hexacarbonyl: influence of potassium on supported tungsten oxide phases, Surf. Sci. 603 (2009) 3041–3048.

[64] E. Krebs, B. Silvi, P. Raybaud, Mixed sites and promoter segregation: a DFT study of the manifestation of Le Chatelier's principle for the Co(Ni)MoS active phase in reaction conditions, Catal. Today 130 (2008) 160–169.

[65] S.L. Gonzaílez-Corteís, Comparing the hydrodesulfurization reaction of thiophene on c-Al_2O_3 supported CoMo, NiMo and NiW sulfide catalysts, React. Kinet. Catal. Lett. 97 (2009) 131–139.

[66] P. Baeza, M.S. Ureta-Zañartu, N. Escalona, J. Ojeda, F.J. Gil-Llambías, B. Delmon, Migration of surface species on supports: a proof of their role on the synergism between CoS_X or NiS_X and MoS_2 in HDS, Appl. Catal. A 274 (2004) 303–309.

[67] Al.A. Pimerzin, P.A. Nikulshin, A.V. Mozhaev, A.A. Pimerzin, A.I. Lyashenko, Investigation of spillover effect in hydrotreating catalysts based on Co_2Mo_{10}-heteropolyanion and cobalt sulphide species, Appl. Catal. B 168 (2015) 396–407.